Low thermal conductivity in ultrathin carbon nanotube (2, 1)

Liyan Zhu[1] & Baowen Li[1,2,3]

[1]Department of Physics, Centre for Computational Science and Engineering, and Graphene Research Center, National University of Singapore, Singapore 117542, Republic of Singapore, [2]NUS Graduate School for Integrative Sciences and Engineering, National University of Singapore, Singapore 117456, Republic of Singapore, [3]Center for Phononics and Thermal Energy Science, School of Physics Science and Engineering, Tongji University, Shanghai 200092, People's Republic of China.

Molecular dynamic simulations reveal that the ultrathin carbon nanotube (CNT) (2, 1) with a reconstructed structure exhibits a surprisingly low thermal conductivity, which is only ∼16–30% of those in regular CNTs, e.g. CNT (2, 2) and (5, 5). Detailed lattice dynamic calculations suggest that the acoustic phonon modes greatly soften in CNT (2, 1) as compared to regular CNTs. Moreover, both phonon group velocities and phonon lifetimes strikingly decrease in CNT (2, 1), which result in the remarkable reduction of thermal conductivity. Besides, isotope doping and chemical functionalization enable the further reduction of thermal conductivity in CNT (2, 1).

Since the discovery of carbon nanotube (CNT)[1], the extraordinary mechanical, physical and chemical properties have made CNTs the most attractive nanomaterials in many aspects and potential applications e.g., electronic devices, gas sensors, solar cells, and textile[2], to name just few of them. Among many characteristic parameters of CNTs, the diameter and chirality directly determine their fundamental properties. Many studies have found that thin CNTs demonstrate much superior properties over the CNTs with large diameters. For example, Poncharal et al. found that the elastic bending modulus of CNTs decrease from 1 to 0.1 TPa as the diameter increases from 8 to 40 nm[3]. Besides, thin CNTs also exhibit much higher carrier mobility than those with large diameters[4]. Furthermore, ultrathin single walled CNT (SWCNT) with a diameter of ∼4 Å shows an exciting superconducting behavior at temperature below 20 K[5]. More importantly, the quantum confinement effect of CNTs, originated from their small diameters, makes thin CNTs a promising nanoreactor to synthesize thin atomic chains[6~8] and a favorable nanocontainer for catalysts[9].

The combination of superior mechanical, physical, and chemical properties in thin CNTs has motivated experimental researchers to narrow the diameters of CNTs. Although it was previously believed that the CNT with diameter less then 3 Å is unstable[10], Zhao[11] and Plank[12] et al. have already successfully synthesized ultrathin CNTs in a narrow CNT with different chiralities, e.g., CNT (2, 2), (3, 1), and (4, 0). Actually, the diameters of CNT (2, 2) and (3, 1) are both less than 3 Å if the C-C bond length is still assumed to be 1.42 Å as that in graphene. So it is of great interest to investigate whether we can push the boundary further to get CNT (2, 1). If CNT (2, 1) still has a tubular structure, its diameter will be as small as ∼2.07 Å assuming the C-C bond length is still 1.42 Å as well. Interestingly, Menendez-Proupinalso et al.[10] predicted that the structure of CNT (2, 1) should show a unique reconstructed shape instead of a smooth graphite cylinder. The reconstructed CNT (2, 1) can be regarded as a twinned double chain connected by bridging C-C bonds (see Figure 1). The whole structure still displays a tubular shape with an outer diameter of 3.2 Å according to first principle density-functional calculations.

On the other hand, the stiff sp^2 C-C bonds in the atomically perfect nanotube cylinders render the CNT with an extremely high thermal conductivity (κ)[13], which is measured to be ∼3400 W/m-K[14] for a SWCNT with a length of 2.6 μm at room temperature. Theoretical study also reveals that the thermal conductivities of thin CNTs increase with the decreasing diameters[15]. Therefore, one might intuitively expect that the ultrathin CNT (2, 1) should also have a giant thermal conductivity because of its extremely small diameter. However, the intriguing reconstructed CNT (2, 1) consists of single, double, and triple C-C bonds alternately arranged, which can also be regarded as a superlattice structure. So it seems that CNT (2, 1) should possess a very low thermal conductivity instead. The deductions from two different points of view lead to exactly opposite outcomes. Which one is correct? To answer this question, we investigate thermal transport properties of CNT (2, 1) using non-equilibrium molecular dynamic (NEMD) simulations in this study. The CNT (2, 2) and (5, 5) are also considered for comparison. The diameters for CNT (2, 2) and (5, 5) are 2.69 and 6.75 Å, respectively. From our simulations, CNT (2, 1) exhibits an exceptionally low thermal conductivity, which is reduced by more than 80% as compared
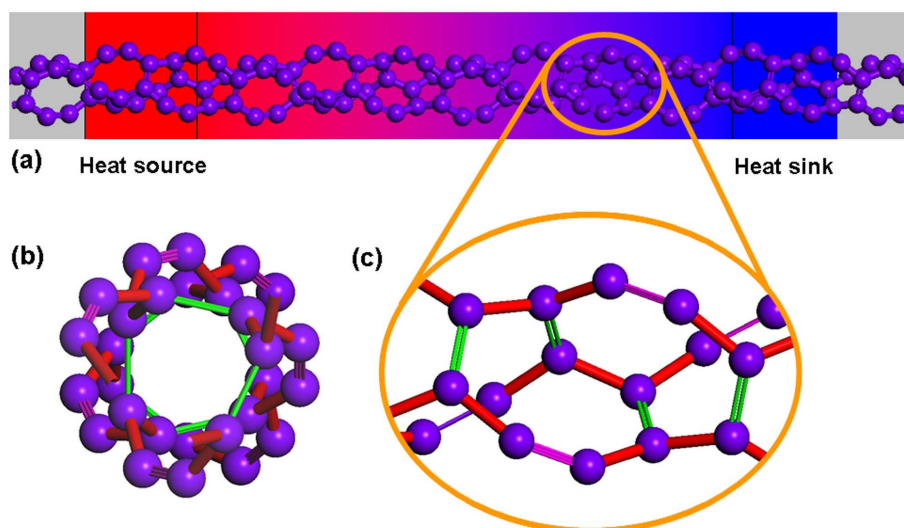
Figure 1 | (a) Schematics of MD simulation domain, (b) cross-sectional view of CNT (2, 1), and (c) zoom-in view of orange circled area of CNT (2, 1) in panel a. Blue balls represent carbon atoms in CNT (2, 1). Red, green, and pink sticks denote single, double, and triple C-C bonds.

to CNT (2, 2). The softening of phonon bands leads to much small phonon group velocities in CNT (2, 1). The superlattice structure, consisting of alternately arranged single, double and triple C-C bonds, makes the phonon scattering rates enhanced noticeably. Thus, the combination of small group velocities and short phonon lifetimes makes the thermal transport properties greatly degraded in CNT (2, 1).

Results and discussion

Figure 2a demonstrates thermal conductivities as a function of the length of CNT (L) for all three systems, i.e., CNT (2, 1), (2, 2), and (5, 5), at 300 K. We firstly discover that the thermal conductivities of all three types of CNTs steadily increase with the increasing length of CNTs from 100 to 500 nm and diverge with respect to length, instead of converging to some finite values, which means that the thermal conductivities of CNTs demonstrate strong length dependence. Furthermore, a closer examination on the thermal conductivities of three-type CNTs implies that they approximately follow a power-law dependence on the length of CNTs, namely, $\kappa \sim L^{\beta}$, where exponent β is a fitting parameter. The best fit gives rise to

exponents 0.45, 0.35, and 0.23 for CNT (2, 1), (2, 2) and (5, 5), respectively. The size dependent thermal conductivity is consistent with previous MD simulations on CNTs by Maruyama[16] and Zhang and Li[17]. It is worth noting that this size dependence of thermal conductivity in CNT has been experimentally confirmed by Chang and co-workers[18]. Besides CNTs, similar size dependence of thermal conductivity is also frequently observed in other low dimensional nano-materials, e.g. graphene nanoribbons[19], silicon nanowires[20], polymers[21] and one-dimensional lattice model[22].

The most striking feature seen from Figure 2a is that the thermal conductivity of CNT (2, 1) is much smaller than CNT (2, 2) and (5, 5). For example, the thermal conductivities are 80.45, 581.14, and 366.70 W/m-K for CNT (2, 1), (2, 2) and (5, 5) with a length of 100 nm, respectively. The thermal conductivity of CNT (2, 1) is about 13.8% of that in CNT (2, 2) and ~21.9% of the value in CNT (5, 5). The inset of Figure 2a summaries the relative thermal conductivity (R) of CNT (2, 1) with respect to CNT (2, 2) and (5, 5) according to the following formula

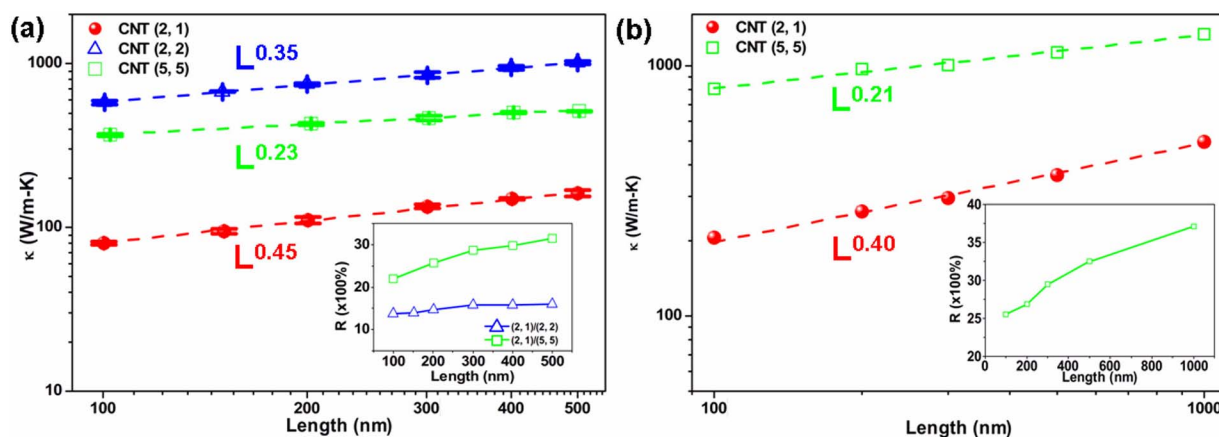$$R = \frac{\kappa_{CNT(2,1)}}{\kappa_{CNT(n,n)}} \times 100\% \quad (n = 2,5). \quad (1)$$

Figure 2 | (a) Thermal conductivities (κ) of CNT (2, 1), (2, 2) and (5, 5) as a function of the length of CNT (L). The inset shows relative thermal conductivity (R) of CNT (2, 1) as compared to CNT (2, 2) (blue open triangle) and (5, 5) (green open square) calculated by using AIREBO potential. (b) Thermal conductivities of CNT (2, 1) and (5, 5) calculated by using optimized Tersoff potential. The inset shows relative thermal conductivity (R) of CNT (2, 1) as compared to CNT (5, 5) (green open square). The dashed curves represent the fitting curve of thermal conductivities by κ ~ L^β. The error bars shown in the panel a represent average standard deviations of six different simulations.
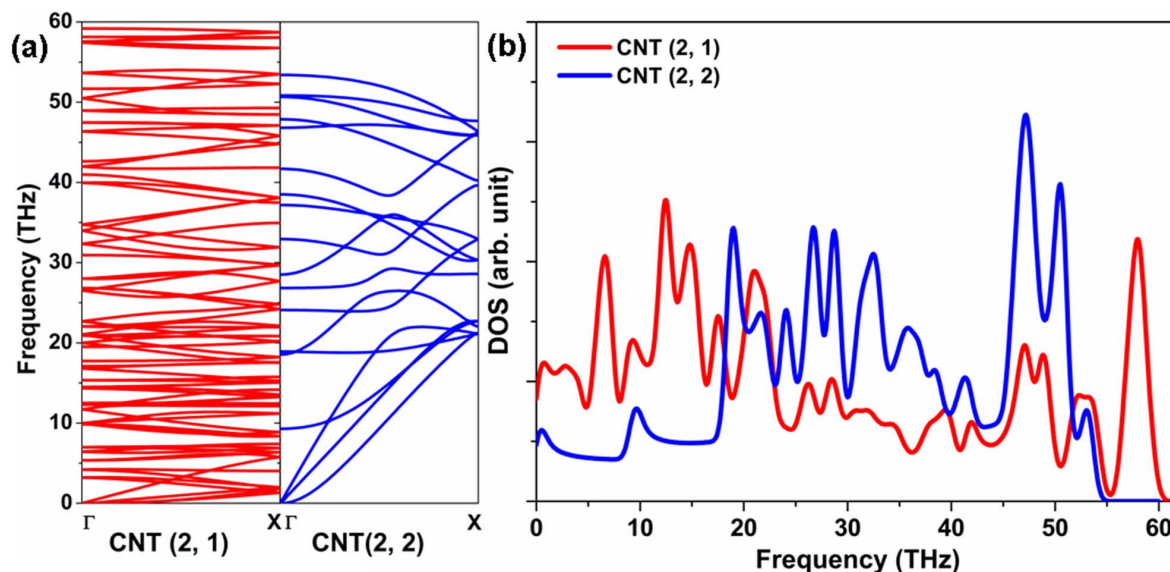
2

Figure 3 | Phonon dispersion (a) and density of states (b) of CNT (2, 1) (red line) and CNT (2, 2) (blue line).

Compared to CNT (2, 2), the thermal conductivity of CNT (2, 1) is reduced by more than 84.0%. More importantly, the reduction in thermal conductivity weakly depends on the length of CNT. However, when compared to CNT (5, 5), the reduction is related to the length of CNT, namely, the reduction gradually decreases from 78.1% to 68.4% as the length of CNT increases from 100 to 500 nm. This is because the length dependence of thermal conductivity of CNT (5, 5) becomes weaker when the length is greater than 400 nm. Similar feature has also been observed in silicon nanowires[20].

However, it is well known that the thermal conductivities computed from classical MD simulations are highly related to the adopted empirical interatomic potential. To verify our results, we also calculate thermal conductivities of CNT (2, 1) and (5, 5) using another widely used empirical potential, that is, the Tersoff type bond order potential with parameters optimized by Lindsay et al.[23]. Here the lengths of CNT (2, 1) and (5, 5) change from 100 to 1000 nm. As shown in Figure 2b, the thermal conductivities of CNT (2, 1) and (5, 5) exhibit a similar dependence on the length. The exponents β for CNT(2, 1) and (5, 5) are 0.40 and 0.21, respectively, which are very close to the values obtained by AIREBO potential. Moreover, the thermal conductivity of CNT (2, 1) still displays a significant reduction as compared to CNT (5, 5) (see Figure 2b). When the length of CNT is 500 nm, the relative thermal conductivity of CNT (2, 1) with respect to CNT (5, 5) is ~32.4% as shown in the inset of Figure 2b, which is close to the value predicted by AIREBO potential, 31.6%. Even though the length of CNT is as long as 1000 nm, the thermal conductivity of CNT (2, 1) decreases by as large as 63% compared to that of CNT (5, 5).

It should be noted that the calculated thermal conductivity by using Tersoff potential is higher than the one obtained from AIREBO potential. Similar phenomenon is also frequently observed in other studies[24]. This is due to that the AIREBO potential yields suppressed phonon dispersion relations which results in underestimated group velocities as compared to the experimental values; while the Tersoff potential with optimized parameters gives rise to improved phonon dispersion and group velocities[23]. However such parameters are only optimized for sp^2 hybridized carbon system, e.g. CNTs and graphene. The improvements on the carbon nanostructure with mixed single, double, and triple C-C bonds are not yet known. Nevertheless, the AIREBO potential explicitly considers σ and π interactions between carbon atoms; and the trend in thermal conductivities predicted from AIREBO potential is in line with that

obtained by using Tersoff potential. So the following analyses are carried out by using AIREBO potential.

To elucidate the underlying mechanism for the significant reduction of thermal conductivity in CNT (2, 1), we next carefully investigate its lattice dynamic properties, and compare them with those in CNT (2, 2). Similar studies can also be applied to CNT (5, 5), which lead to the same conclusions. Figure 3a shows the phonon dispersions of both CNT (2, 1) and (2, 2), in which eigen-frequencies are obtained by diagonalizing dynamic matrix using PHONOPY[25]. From the phonon dispersions shown in Figure 3a, we can clearly find that the acoustic phonon modes dramatically soften in CNT (2, 1), of which the reason will be explained in more details later. The softening of acoustic phonon can also be inferred from density of states (DOS) as plotted in Figure 3b. Apparently, the DOS of CNT (2, 1) at low-frequency region, i.e., < 18 THz, is much larger than that of CNT (2, 2), which is exactly due to the softening of acoustic phonon modes in CNT (2, 1). In the intermediate and high frequency region, the DOS of CNT (2, 1) becomes smaller than that of CNT (2, 2).

The direct consequence of phonon softening is the reduction in group velocities. To quantitatively compare the group velocities (v_g) of phonons in CNT (2, 1) and (2, 2), we calculate them according to Hellmann-Feynman theorem,

$$\mathbf{v}_g = \frac{1}{2\omega} \mathbf{e}_{ph}^{\mathrm{T}} \frac{\partial \mathbf{D}}{\partial \mathbf{q}} \mathbf{e}_{ph}, \quad (2)$$

where $\mathbf{D}$, $\mathbf{e}_{ph}$, and ω are dynamic matrix, phonon eigenvector, and eigen-frequency, respectively. The obtained group velocities of phonons in both CNT (2, 1) and CNT (2, 2) are drawn in Figure 4a. In the intermediate and high frequency region, i.e., >18 THz, the phonon group velocities in CNT (2, 1) are comparable to or slight smaller than those in CNT (2, 2). But in the low-frequency region, the group velocities of phonons in CNT (2, 1) are much smaller than those in CNT (2, 2), for example, the sound velocity of longitudinal acoustic (LA) phonon is about ~22 km/s in CNT (2, 2), while it is plummeted to ~15 km/s in CNT (2, 1). The reduction of group velocities will strongly lower the thermal conductivity. The contribution of phonon mode (**q**, ν) to the total thermal conductivity can be expressed as

$$\kappa = \frac{1}{N} \sum_{\mathbf{q}} \sum_{\upsilon} C_{ph}(\mathbf{q}, \upsilon) \mathbf{v}_g^2(\mathbf{q}, \upsilon) \tau(\mathbf{q}, \upsilon) \quad (3)$$

where $C_{ph}(\mathbf{q}, \nu)$, $\mathbf{v}_g(\mathbf{q}, \nu)$ and $\tau(\mathbf{q}, \nu)$ are volumetric specific heat, group velocity, and lifetime of the phonon mode (**q**, ν) (**q** and ν
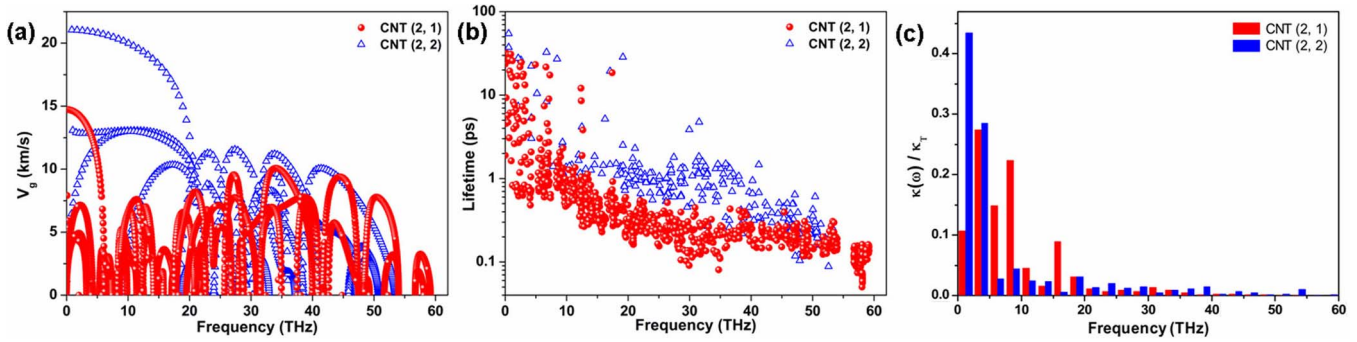
Figure 4 | (a) Group velocities, (b) phonon lifetimes, and (c) frequency resolved thermal conductivity distributions in CNT (2, 1) and (2, 2).

denote the phonon wavevector and the index of phonon branch, respectively), respectively; and N is the total number of q points. Considering the fact that the acoustic phonon modes are usually major energy carriers in thermal transport, the reduced group velocities of acoustic phonon modes in CNT (2, 1) will remarkably reduce its thermal conductivity.

Another factor strongly affecting thermal conductivity is the phonon lifetime, which can be calculated from spectra energy density (SED, $\Phi(\mathbf{q},v,\omega)$) using the following formula[26],

$$\Phi(\mathbf{q},v,\omega) = \lim_{T \to \infty} \frac{1}{2T} \left| \frac{1}{\sqrt{2\pi}} \int_0^T \sum_{\mathbf{R},i} \sqrt{\frac{m_b}{N}} \exp\{i[\mathbf{q}\cdot\mathbf{r}(\mathbf{R},0)-\omega t]\}\mathbf{e}_b^*(\mathbf{q},v)\cdot\dot{\mathbf{u}}(\mathbf{R},b,t)dt \right|^2,$$
(4)

Where b is the index of basis atom in the primitive cell of CNTs; $\mathbf{R}$ is a lattice vector connecting primitive cells; m_b is the mass of atom b. N is the total number of cells employed in MD simulations. $\dot{\mathbf{u}}(\mathbf{R},b,t)$ is the velocity of atom b in cell $\mathbf{R}$ at time t. $\mathbf{e}_b^*(\mathbf{q},v)$ is the complex conjugate of the eigenvector associated with atom b for the phonon mode $(\mathbf{q}, v)$. $\mathbf{r}(\mathbf{R}, 0)$ represents the equilibrium position of unit cell $\mathbf{R}$.

SED should satisfy a Lorenzian distribution[26], namely,

$$\Phi(\mathbf{q},v,\omega) = C \frac{\Gamma(\mathbf{q},v)/\pi}{[\omega - \omega(\mathbf{q},v)]^2 + \Gamma^2(\mathbf{q},v)},$$
(5)

where $\omega(\mathbf{q}, v)$ is the eigen-frequency for the phonon mode $(\mathbf{q}, v)$ and $\Gamma(\mathbf{q}, v)$ corresponds to the half width at half maximum of SED. After fitting SED with a Lorenzian function, we can get the phonon lifetime (τ) through $\tau = 1/[2\Gamma(\mathbf{q}, v)]$.

Phonon lifetimes as a function of frequency are presented in Figure 4b for both CNT (2, 1) and (2, 2). Generally, the phonon lifetimes exhibit a quick decline when the frequency increases. This is because phonon scattering events must satisfy both moment and energy conservation laws. The phonon modes close to Brillouin zone center with low frequencies have few probabilities to fulfill both requirements. So the scattering rate generally increases with the increasing frequency. Consequently, the phonon lifetime would roughly decreases with the phonon frequency increases, which has been suggested to follow a power law $\sim\omega^{-\alpha}$ [27]. Another noticeable feature observed from Figure 4b is that the phonon lifetimes in CNT (2, 1) are smaller than CNT (2, 2) overall. Specifically speaking, the phonon lifetimes in CNT (2, 2) are about 40–60 ps for the very low-frequency phonons, i.e., <1 THz; but they are less than 40 ps in CNT (2, 1). The decrease of phonon lifetimes is even more apparent for phonon modes with frequencies ranging between 10–40 THz in CNT (2, 1), as compared to CNT (2, 2). As a consequence, the CNT (2, 1) possesses a much smaller thermal conductivity than CNT (2, 2).

Having the knowledge of phonon modes resolved group velocities and lifetimes, we can obtain the contribution of each phonon mode to the total thermal conductivity. We plot the frequency resolved thermal conductivity distribution ($\kappa(\omega)$) normalized by total thermal conductivity (κ_T) in Fig. 4c. In CNT (2, 2), the low-frequency acoustic phonon modes dominate the thermal conductivity. However, the contribution of low-frequency phonons to total thermal conductivity obviously decreases in CNT (2, 1); while the medium-frequency phonons have greatly enhanced contribution to thermal conductivity as compared to CNT (2, 2). This is because the acoustic phonon modes become softened and their lifetimes shortened. So their contributions to thermal transport also become smaller. Besides, we find the mean free path of low-frequency phonons in CNT (2, 1) and (2, 2) are longer than 150 and 600 nm, respectively, which are comparable to the size of system employed in MD simulations. Therefore, such phonons transport ballistically along the system. More importantly, more phonons with long mean free path will be excited as the length of CNTs increases[28]. These two factors are the reasons why the thermal conductivity showing a power law dependence on the length of CNTs.

So far the lattice dynamic properties of CNT (2, 1) and (2, 2) have been systematically investigated. We have identified that the degraded thermal transport ability in CNT (2, 1) is due to the greatly lowered phonon group velocities and phonon lifetimes. The cause of reduction in the latter two quantities can be traced back to the peculiar structure of CNT (2, 1). Generally, the CNT is regarded as a rolling cylinder of graphene sheet with uniform conjugate C-C bonds. The strong σ bonds in the wall make the CNT of high stiffness. However, the unique reconstruction occurs in CNT (2, 1), in which the single, double and triple C-C bonds stack alternately. So the carbon atoms in CNT (2, 1) can be divided into two categories, i.e., two- and three-coordinated carbon atoms which will be named as C_2 and C_3 hereafter. Hence the CNT (2, 1) can be regarded as a superlattice composed of C_2 and C_3 periodically. The two types of atoms have distinctly different local DOS as shown in Figure 5a. When frequency is less than 20 THz, the local DOS of C_2 is much higher than that of C_3. But the situation is exactly reversed when the frequency is larger than 20 THz. The local DOS of C_2 is greatly suppressed and becomes smaller than that of C_3 for frequencies between 20 and 55 THz. However, all carbon atoms in CNT (2, 2) have the same local DOS due to its uniform structure. The dramatic change in local DOS of C_2 and C_3 in CNT (2, 1) can be well understood from mode weight factor (f), which is defined as[29–32],

$$f(\mathbf{q},v) = \sum_i \mathbf{e}_i^*(\mathbf{q},v)\bullet\mathbf{e}_i(\mathbf{q},v),$$
(6)

where the summation runs over C_2 (C_3) type atoms. This quantity, varying from 0 to 1, evaluates the relative contribution from each type of atoms to each eigenmode. Figure 5b compares the mode weight factor of both C_2 and C_3 for all phonon modes. Apparently, most phonon modes with frequencies less than 20 THz are majorly contributed by C_2. But the contributions from C_2 become much smaller than those from C_3 for phonon modes with frequency higher than 20 THz. The distinctive mismatch between C_2 and C_3 type
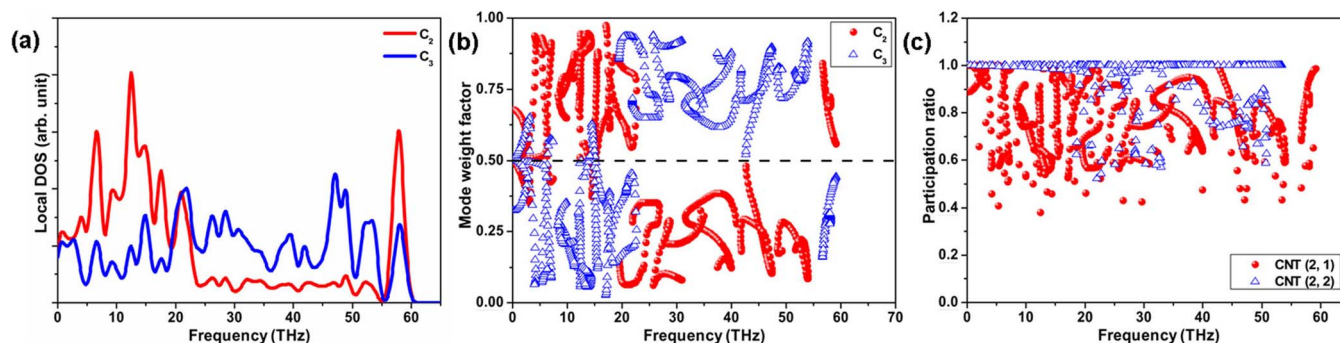
Figure 5 | (a) Local DOS of two- (red line) and three-coordinated (blue line) carbon atoms in CNT (2, 1). (b) Phonon mode weight factors of two- (red ball) and three-coordinated (blue open triangle) carbon atoms in CNT (2, 1). (c) Participation ratio of each phonon mode in CNT (2, 1) (red ball) and CNT (2, 2) (blue open triangle).

atoms leads to the strong softening of phonon modes. Accordingly, the group velocities of low-frequency phonons remarkably decrease. It also makes the phonon scattering rate greatly enhanced in CNT (2, 1), which results in short phonon lifetimes in CNT (2, 1) consequently. These combined factors reduce the thermal conductivity of CNT (2, 1) greatly. Furthermore, the mismatched vibration properties between C_2 and C_3 will also induce phonon localization effect, which could be quantitatively reflected by the participation ratio (P) of each eigenmode[29,30,32,33]. The definition is,

$$P(\mathbf{q},v)^{-1} = N \sum_i [\mathbf{e}_i^*(\mathbf{q},v) \bullet \mathbf{e}_i(\mathbf{q},v)]^2, \qquad (7)$$

where N is the total number of atoms. The summation runs over all atoms in a unit cell. The participation ratio, changing from 1/N to 1, estimates the fraction of atoms participating each vibrational eigenmode. It is a useful measure of spatial localization of eigenmodes. As clearly shown in Figure 5c, the low-frequency phonon modes in CNT (2, 2), corresponding to a participation ratio of 1, are almost perfectly delocalized. The phonon mode shows slight localization, only when the frequency is greater than ~20 THz. But in CNT (2, 1), the participation ratios range from 0.4 to 1.0, from the lowest to highest phonon modes. The enhanced phonon localization definitely inhibits the thermal transport in CNT (2, 1).

Moreover, previous studies have already found that the thermal conductivity can be effectively reduced by isotope doping[17,34,35]. Besides, high concentration vacancy defects[36] and covalent modification[37] of CNTs with molecules also reduce the thermal conductivity by 80–90%. Apparently, the reduction of thermal conductivity in CNT (2, 1) is already comparable to CNTs with vacancy defects and chemical modification at a high concentration. Moreover, we expect a further decrease of thermal conductivity in CNT (2, 1) by isotope doping and/or chemical functionalization. However, the isotope doping usually has a prominent role in suppressing the phonon lifetimes of high frequency phonon modes[38]. While the lifetimes of high frequency phonon modes in CNT (2, 1) are already shortened by its supperlattice-like structure. Thus, thermal conductivity of CNT (2, 1) can be reduced up to ~20% only by isotope doping. But the hydrogenated CNT (2, 1) exhibits an additional ~65% reduction in thermal conductivity as compared to pristine CNT (2, 1). Most importantly, the thermal conductivity of fully hydrogenated CNT (2, 1) only weakly depends on its length, namely, the thermal conductivities are 28.3, 33.4, and 34.5 W/m-k for the fully hydrogenated CNT (2, 1) with a length of 100, 200, and 300 nm, respectively. However the reason why the length dependence of hydrogenated CNT (2, 1) becomes much weak is beyond the scope to current study.

Conclusion

In summary, we have carried out systematic MD simulations and lattice dynamic calculations of the thermal properties of ultrathin

CNT (2, 1). The thermal conductivity of CNT (2, 1) decreases by more than 80% with respect to CNT (2, 2) and around 70% to CNT (5, 5). By examining phonon dispersion and density of states, we find that the acoustic phonon modes in CNT (2, 1) greatly soften compared to CNT (2, 2). The softening of acoustic phonon modes leads to small group velocities, which is validated by numerical calculations. Besides, the phonon lifetimes also show a great reduction in CNT (2, 1) due to the enhanced phonon scattering. These two combined factors account for the significant reduction of thermal conductivity in CNT (2, 1). Actually this reduction in thermal conductivity is comparable to the hydrogen modified CNTs[37] and CNTs with vacancy defects at a high concentration[36]. The thermal conductivity of CNT (2, 1) can be further reduced by isotope doping and chemical functionalization[37].

Methods

All molecular dynamic (MD) simulations are carried out using Large-scale Atomic/Molecular Massively Parallel Simulator (LAMMPS)[39]. We use the adaptive intermolecular reactive bond order (AIREBO) potential[40] to model the covalent bonding interactions between carbon atoms in CNTs. Equations of motion are integrated by the velocity verlet algorithm with a time step of 0.5 fs. We firstly equilibrate the whole system at the desired temperature (300 K) using canonical ensemble with a Langevine thermostate[41] for 0.5 ns. Then a microcanonical ensemble MD simulation runs for another 50 ns. In this stage of simulation, we divide the system into five segments as shown in Figure 1 in order to calculate thermal conductivity using non-equilibrium method. The left and right ends of CNTs are fixed as shown in the grey area of Figure 1a. Another two segments adjacent to the two fixed ends serve as heat source and heat sink whose temperatures are fixed at 310 K and 290 K in the rest simulations, respectively. The lengths of heat source and heat sink segments set to be ~10 Å. The thermal conductivity (κ) is computed using Fourier's law, namely,

$$\kappa = \frac{J}{A\nabla T}, \qquad (8)$$

where J is the heat current transported through CNTs and can be calculated as J = dE/dt. Here E is the energy flowing either out of heat source or into heat sink. The symbol A in Eq. 8 represents the cross-sectional area of CNT. For CNT (2, 1) and (5, 5) the cross-sectional area is calculated as A = πRh where R and h mean the diameter of CNT and the thickness of its wall which is assume to be the interlayer spacing in graphite, i.e., 3.35 Å. As for CNT (2, 2), the cross-sectional area is computed as A = π(R+h)²/4 since its diameter is less than 3.35 Å. The exact values of A for CNT (2, 1), (2, 2), and (5, 5) are 36.19, 28.08, 71.08 Å², respectively. The constant heat current can be achieved when the system reaches a steady state. The term ∇T in Eq. 8 is the temperature gradient, which is obtained by fitting the time averaged temperature profile in the central linear segment by a linear function. The lengths of CNTs vary from 100 to 500 nm. For each length, the final thermal conductivity is averaged over six independent MD runs with different initial conditions. Moreover, we also employ another widely used bond order potential, i.e., optimized Tersoff potential[23] to verify whether the trend in thermal conductivities obtained with AIREBO. It should be noted that the lengths of CNTs change from 100 to 1000 nm when optimized Tersoff potential is adopted.

1. Iijima, S. Helical microtubules of graphitic carbon. *Nature* **354**, 56–58 (1991).
2. Endo, M., Strano, M. & Ajayan, P. in *Carbon Nanotubes* Vol. 111 *Topics in Applied Physics* Ch. 2, 13–61 (Springer Berlin Heidelberg, 2008).

3. Poncharal, P., Wang, Z. L., Ugarte, D. & de Heer, W. A. Electrostatic Deflections and Electromechanical Resonances of Carbon Nanotubes. *Science* **283**, 1513–1516 (1999).

4. Asada, Y., Nihey, F., Ohmori, S., Shinohara, H. & Saito, T. Diameter-Dependent Performance of Single-Walled Carbon Nanotube Thin-Film Transistors. *Adv. Mater.* **23**, 4631–4635 (2011).

5. Tang, Z. K. *et al.* Superconductivity in 4 Angstrom Single-Walled Carbon Nanotubes. *Science* **292**, 2462–2465 (2001).

6. Fujimori, T. *et al.* Conducting linear chains of sulphur inside carbon nanotubes. *Nat. Commun.* **4**, 2162 (2013).

7. Miyamoto, Y., Rubio, A., Blase, X., Cohen, M. L. & Louie, S. G. Ionic Cohesion and Electron Doping of Thin Carbon Tubules with Alkali Atoms. *Phys. Rev. Lett.* **74**, 2993–2996 (1995).

8. Shi, L. *et al.* Ultra-thin double-walled carbon nanotubes: A novel nanocontainer for preparing atomic wires. *Nano Res.* **4**, 759–766 (2011).

9. Zhang, F. *et al.* Tuning the redox activity of encapsulated metal clusters via the metallic and semiconducting character of carbon nanotubes. *Proc. Natl. Acad. Sci. U.S.A.* **110**, 14861–14866 (2013).

10. Menéndez-Proupin, E., Montero-Alejo, A. L. & García de la Vega, J. M. Ultrathin Carbon Nanotube With Single, Double, and Triple Bonds. *Phys. Rev. Lett.* **109**, 105501 (2012).

11. Zhao, X. *et al.* Smallest Carbon Nanotube Is 3 Å in Diameter. *Phys. Rev. Lett.* **92**, 125502 (2004).

12. Plank, W. *et al.* Electronic Structure of Carbon Nanotubes with Ultrahigh Curvature. *ACS Nano* **4**, 4515–4522 (2010).

13. Berber, S., Kwon, Y.-K. & Tománek, D. Unusually High Thermal Conductivity of Carbon Nanotubes. *Phys. Rev. Lett.* **84**, 4613–4616 (2000).

14. Pop, E., Mann, D., Wang, Q., Goodson, K. & Dai, H. Thermal Conductance of an Individual Single-Wall Carbon Nanotube above Room Temperature. *Nano Lett.* **6**, 96–100 (2005).

15. Lindsay, L., Broido, D. A. & Mingo, N. Diameter dependence of carbon nanotube thermal conductivity and extension to the graphene limit. *Phys. Rev. B* **82**, 161402 (2010).

16. Maruyama, S. A molecular dynamics simulation of heat conduction in finite length SWNTs. *Phys. B* **323**, 193–195 (2002).

17. Zhang, G. & Li, B. Thermal conductivity of nanotubes revisited: Effects of chirality, isotope impurity, tube length, and temperature. *J. Chem. Phys.* **123**, 114714 (2005).

18. Chang, C. W., Okawa, D., Garcia, H., Majumdar, A. & Zettl, A. Breakdown of Fourier's Law in Nanotube Thermal Conductors. *Phys. Rev. Lett.* **101**, 075903 (2008).

19. Nika, D. L., Askerov, A. S. & Balandin, A. A. Anomalous Size Dependence of the Thermal Conductivity of Graphene Ribbons. *Nano Lett.* **12**, 3238–3244 (2012).

20. Yang, N., Zhang, G. & Li, B. Violation of Fourier's law and anomalous heat diffusion in silicon nanowires. *Nano Today* **5**, 85–90 (2010).

21. Liu, J. & Yang, R. Length-dependent thermal conductivity of single extended polymer chains. *Phys. Rev. B* **86**, 104307 (2012).

22. Liu, S., Xu, X. F., Xie, R. G., Zhang, G. & Li, B. W. Anomalous heat conduction and anomalous diffusion in low dimensional nanoscale systems. *Eur. Phys. J. B* **85**, 1–20 (2012).

23. Lindsay, L. & Broido, D. A. Optimized Tersoff and Brenner empirical potential parameters for lattice dynamics and phonon thermal transport in carbon nanotubes and graphene. *Phys. Rev. B* **81**, 205441 (2010).

24. Li, X., Chen, J., Yu, C. & Zhang, G. Comparison of isotope effects on thermal conductivity of graphene nanoribbons and carbon nanotubes. *Appl. Phys. Lett.* **103**, 013111 (2013).

25. Togo, A., Oba, F. & Tanaka, I. First-principles calculations of the ferroelastic transition between rutile-type and $CaCl_2$-type SiO_2 at high pressures. *Phys. Rev. B* **78**, 134106 (2008).

26. Larkin, J. M., Turney, J. E., Massicotte, A. D., Amon, C. H. & McGaughey, A. J. H. Comparison and Evaluation of Spectral Energy Methods for Predicting Phonon Properties. *J. Comput. Theor. Nanos.* **11**, 249–256 (2014).

27. Holland, M. G. Analysis of Lattice Thermal Conductivity. *Phys. Rev.* **132**, 2461–2471 (1963).

28. Salaway, R. N. & Zhigilei, L. V. Molecular dynamics simulations of thermal conductivity of carbon nanotubes: Resolving the effects of computational parameters. *Int. J. Heat Mass Transfer.* **70**, 954–964 (2014).

29. Allen, P. B., Feldman, J. L., Fabian, J. & Wooten, F. Diffusons, locons and propagons: Character of atomic vibrations in amorphous Si. *Philos. Mag. B* **79**, 1715–1731 (1999).

30. Bodapati, A., Schelling, P. K., Phillpot, S. R. & Keblinski, P. Vibrations and thermal transport in nanocrystalline silicon. *Phys. Rev. B* **74**, 245207 (2006).

31. Hu, M. & Poulikakos, D. Si/Ge Superlattice Nanowires with Ultralow Thermal Conductivity. *Nano Lett.* **12**, 5487–5494 (2012).

32. Chen, J., Zhang, G. & Li, B. Phonon coherent resonance and its effect on thermal transport in core-shell nanowires. *J. Chem. Phys.* **135**, - (2011).

33. Hu, M., Giapis, K. P., Goicochea, J. V., Zhang, X. & Poulikakos, D. Significant Reduction of Thermal Conductivity in Si/Ge Core−Shell Nanowires. *Nano Lett.* **11**, 618–623 (2010).

34. Chang, C. W. *et al.* Isotope Effect on the Thermal Conductivity of Boron Nitride Nanotubes. *Phys. Rev. Lett.* **97**, 085901 (2006).

35. Zhang, G. & Li, B. Impacts of doping on thermal and thermoelectric properties of nanomaterials. *Nanoscale* **2**, 1058–1068 (2010).

36. Park, J., Bifano, M. F. P. & Prakash, V. Sensitivity of thermal conductivity of carbon nanotubes to defect concentrations and heat-treatment. *J. Appl. Phys.* **113**, 034312 (2013).

37. Padgett, C. W. & Brenner, D. W. Influence of Chemisorption on the Thermal Conductivity of Single-Wall Carbon Nanotubes. *Nano Lett.* **4**, 1051–1053 (2004).

38. Zhang, G. & Zhang, Y.-W. Thermal conductivity of silicon nanowires: From fundamentals to phononic engineering. *Phys. Status Solidi RRL* **7**, 754–766 (2013).

39. Plimpton, S. Fast Parallel Algorithms for Short-Range Molecular Dynamics. *J. Comput. Phys.* **117**, 1–19 (1995).

40. Stuart, S. J., Tutein, A. B. & Harrison, J. A. A reactive potential for hydrocarbons with intermolecular interactions. *J. Chem. Phys.* **112**, 6472–6486 (2000).

41. Schneider, T. & Stoll, E. Molecular-dynamics study of a three-dimensional one-component model for distortive phase transitions. *Phys. Rev. B* **17**, 1302–1322 (1978).

Acknowledgments

Author contributions

L.Z. designed the project, performed the calculations and drafted the paper. B.L. supervised the project, discussed the results and revised the manuscript.

Additional information

Competing financial interests: The authors declare no competing financial interests.

How to cite this article: Zhu, L.Y. & Li, B.W. Low thermal conductivity in ultrathin carbon nanotube (2, 1). *Sci. Rep.* **4**, 4917; DOI:10.1038/srep04917 (2014).